crystals

MDPI

Article

Macroscopic Dehydration Control of $ZnSO_4 \cdot 7H_2O$: Infrared and Raman Spectra of $ZnSO_4$ Hydrates

Chengang Ding [1,2], Wenling Zheng [2,3], Rongrong Xue [2,*] and Fenghua Chen [2,*]

[1] College of Material Engineering, Fujian Agriculture and Forestry University, Fuzhou 350100, China; 5221038049@fafu.edu.cn
[2] School of Resources and Chemical Engineering, Sanming University, Sanming 365004, China; 220427153@fzu.edu.cn
[3] School of Chemical Engineering, Fuzhou University, Fuzhou 350116, China
* Correspondence: rongrongxue@fjsmu.edu.cn (R.X.); fenghuachen@fjsmu.edu.cn (F.C.)

Abstract: With microscopic thermogravimetric analysis, it is difficult to prepare metastable intermediate phases with precise water contents during the dehydration process of hydrates, making it a challenge to acquire their related spectra. The gradual dehydration process of $ZnSO_4 \cdot 7H_2O$ proceeds through $7 \rightarrow 6 \rightarrow 4 \rightarrow 1 \rightarrow 0$. Vibrational spectra of $ZnSO_4$ hydrates, especially $ZnSO_4 \cdot 6H_2O$ and $ZnSO_4 \cdot 4H_2O$, have not been previously reported. By macroscopic thermogravimetric analysis of $ZnSO_4 \cdot 7H_2O$, the dehydration process can be precisely controlled to produce a variety of $ZnSO_4$ hydrates with specific water contents. In this study, powder X-ray diffraction confirmed the purities of $7H_2O$, $6H_2O$, $4H_2O$, $1H_2O$ and anhydrous $ZnSO_4$. IR and Raman spectra of $ZnSO_4$ hydrates were obtained and compared for the first time. Spectroscopic and crystallographic analysis revealed that structural similarity plays a key role in the $7 \rightarrow 6 \rightarrow 4 \rightarrow 1 \rightarrow 0$ dehydration process. Macroscopic thermogravimetric analysis combined with powder X-ray diffraction is a valuable method for investigating the intermediate phases in the hydrate dehydration process.

Keywords: $ZnSO_4 \cdot 7H_2O$ dehydration; macroscopic thermogravimetric analysis; IR and Raman spectra; principle of similarity

check for updates

Academic Editor: Juan Ángel Sans

Received: 18 February 2025
Revised: 26 February 2025
Accepted: 3 March 2025
Published: 10 March 2025

Citation: Ding, C.; Zheng, W.; Xue, R.; Chen, F. Macroscopic Dehydration Control of $ZnSO_4 \cdot 7H_2O$: Infrared and Raman Spectra of $ZnSO_4$ Hydrates. *Crystals* **2025**, *15*, 257. https://doi.org/10.3390/cryst15030257

Copyright: © 2025 by the authors. Licensee MDPI, Basel, Switzerland. This article is an open access article distributed under the terms and conditions of the Creative Commons Attribution (CC BY) license (https://creativecommons.org/licenses/by/4.0/).

1. Introduction

Inorganic salt hydrates can lose their crystallized water with increasing temperature or decreasing humidity [1–3]. The dehydration process can involve multiple steps before the hydrate reaches a thermodynamically stable state [4–6]. The dehydration and reverse processes of inorganic salt hydrates involve the absorption and release of a large amount of energy, which makes inorganic salt hydrates a potential candidate for thermal energy storage and release [7,8]. Understanding the multi-step dehydration process of inorganic salt hydrates is of great significance for understanding their fundamental properties and their applications as energy storage materials.

The main research methods for hydrate dehydration are X-ray diffraction (XRD) and microscopic thermal analysis (TA) techniques [9–12], such as thermogravimetric analysis (TGA), differential scanning calorimetry (DSC) and differential thermal analysis (DTA). It is a challenge to combine powder XRD (PXRD) and microscopic TA, even in ex situ conditions, for the following reasons. (1) The atmosphere for PXRD testing is usually air at ambient humidity, and that for microscopic TA is usually dry air or N_2. These different atmospheres can make it difficult to discern changes in water content in ex situ conditions. (2) The sample mass for microscopic TA is milligram-scale, which is usually not large

enough for PXRD, and is not easily transferred from the crucible. (3) Some inorganic salt hydrates do not have a clear dehydration step, and it is difficult to obtain intermediate phases with precise water contents in microscopic TA. For inorganic salt hydrates with clear dehydration steps, these problems are not critical. For example, the dehydration process of $CuSO_4 \cdot 5H_2O$, a common standard material for calibrating DSC-TGA instruments [13], is $5 \rightarrow 3 \rightarrow 1 \rightarrow 0$, with clear dehydration steps [14]. The stability of $CuSO_4 \cdot 3H_2O$, $CuSO_4 \cdot H_2O$ and anhydrous $CuSO_4$ is sufficient in air. Thus, IR [15,16] and Raman [17] spectra of various $CuSO_4$ hydrates have been reported to align well with microscopic TGA. However, in the case of $ZnSO_4 \cdot 7H_2O$ (Table 1), the gradual dehydration process proceeds through $7 \rightarrow 6 \rightarrow 4 \rightarrow 1 \rightarrow 0$, which has been confirmed by microscopic TA [18] and diffraction methods [19,20]. Dehydration from $ZnSO_4 \cdot 7H_2O$ to $ZnSO_4 \cdot H_2O$ is only a continuous process in microscopic TGA, making it challenging to isolate intermediate products with precise compositions. The single-crystal data of $ZnSO_4 \cdot 7H_2O$, $6H_2O$, $4H_2O$, $1H_2O$ and anhydrous $ZnSO_4$ have been reported (Table 2), but the IR and Raman spectra of $ZnSO_4 \cdot 6H_2O$ and $ZnSO_4 \cdot 4H_2O$ have not been reported.

Table 1. Some reported dehydration processes of $ZnSO_4 \cdot 7H_2O$.

Year	Process	Method	Refs.
1953	$7 \rightarrow 6 \rightarrow 1$	DTA	[21]
1955	$7 \rightarrow 1 \rightarrow$ amorphous	XRD (vacuum)	[22]
1969	$7 \rightarrow 6 \rightarrow 1$	TGA-DTA	[23]
1975	$7 \rightarrow 6 \rightarrow 4 \rightarrow 1$	DSC, DTA, TGA	[18]
1982	$7 \rightarrow 6 \rightarrow 1$	Calorimetric containers of fused silica	[24]
1997	$7 \rightarrow 6 \rightarrow 1$	DTA, DTG, TG (5 K·min^{-1}, 20–1000 °C)	[25]
2005	$7 \rightarrow 6 \rightarrow 4 \rightarrow 1$	Neutron PXRD and single-crystal XRD	[19]
2006	$7 \rightarrow 6 \rightarrow 1 \rightarrow 0$	DTA, TG (5 K·min^{-1})	[26]
2011	$7 \rightarrow 1$	TGA-DTA (30 °C·min^{-1} in air)	[27]
2012	$7 \rightarrow 6 \rightarrow 4 \rightarrow 1$	In situ diffraction	[20]
2013	$7 \rightarrow 1 \rightarrow 0$	TPD-MS-SMB	[28]
2014	$7 \rightarrow 6 \rightarrow 1$	TG-DTA, fluidized bed drier	[29]
2014	$7 \rightarrow 6 \rightarrow 1 \rightarrow X \rightarrow 0$	TG-DTA (5 K·min^{-1}, 25–1100 °C, air)	[30]
2018	$7 \rightarrow 6 \rightarrow 1$	Water vapor sorption analyzer, microbalance	[31]
2020	$7 \rightarrow 5 \rightarrow 1$	DSC-TG (1 K·min^{-1}, 25–150 °C, N_2)	[32]
2022	$7 \rightarrow 6 \rightarrow 1$	All-fiber terahertz time-domain spectroscopy	[33]
2022	$7 \rightarrow 6 \rightarrow 1$	TGA (10 K·min^{-1}, 25–1000 °C, N_2)	[34]

Table 2. Unit cell parameters of $ZnSO_4 \cdot 7H_2O$, $ZnSO_4 \cdot 6H_2O$, $ZnSO_4 \cdot 4H_2O$, $ZnSO_4 \cdot H_2O$ and anhydrous $ZnSO_4$.

	$7H_2O$	$6H_2O$	$4H_2O$	H_2O	Anhydrous
Year	1959	1979	2001	1991	1978
ICSD No.	107287	41708	280878	71348	2456
System	Orthorhombic	Monoclinic	Monoclinic	Monoclinic	Cubic
Space Group	$P2_12_12_1$	C2/c	$P2_1/n$	C2/c	F-43m
a (Å)	11.779	9.981	5.904	6.925	7.176
b (Å)	12.050	7.250	13.519	7.591	7.176
c (Å)	6.822	24.280	7.883	7.635	7.176
α (°)	90	90	90	90	90
β (°)	90	98.45	90.26	118.19	90
γ (°)	90	90	90	90	90

Macroscopic TGA is widely used for determining the moisture content in food [35,36]. Different from TGA, DSC and DTA, macroscopic TGA is operated with samples of mass in the order of grams under air conditions. This method enables the dehydration process to be interrupted at any time and the product to be transferred. Using grams of sample can enhance the reproducibility of the experiment and the storage stability of the sample, which is conducive to the combination of this method with PXRD and spectroscopic analysis.

In this work, macroscopic TGA was successfully used for the preparation of various $ZnSO_4$ hydrates with precise water contents. PXRD confirmed that the prepared $ZnSO_4{\cdot}7H_2O$, $ZnSO_4{\cdot}6H_2O$, $ZnSO_4{\cdot}H_2O$ and anhydrous $ZnSO_4$ are pure and $ZnSO_4{\cdot}4H_2O$ has high purity with a small amount of $ZnSO_4{\cdot}6H_2O$ and $ZnSO_4{\cdot}H_2O$. IR and Raman spectra of the various $ZnSO_4$ hydrates were obtained for the first time. Spectroscopic and crystallographic analysis indicate that the gradual dehydration of $ZnSO_4{\cdot}7H_2O$ through $7 \rightarrow 6 \rightarrow 4 \rightarrow 1 \rightarrow 0$ is consistent with the principle of structural similarity. The combination of macroscopic TGA analysis and PXRD has advantages in preparing the intermediate phases with precise water contents, determining the polymorphs of the intermediate phases and obtaining the spectra of the intermediate phases in the dehydration process.

2. Materials and Methods

2.1. Materials

Zinc sulfate heptahydrate ($ZnSO_4{\cdot}7H_2O$, 99.5%) was bought from Xilong Chemical Co. Raw $ZnSO_4{\cdot}7H_2O$ would dehydrate during storage, and the fresh $ZnSO_4{\cdot}7H_2O$ used in this work was prepared by the following method. A total of 5 g of ground raw $ZnSO_4{\cdot}7H_2O$ was totally dissolved in 10 mL of water, and then the solution was evaporated in air (26 °C, ~60% humidity) until most of the solution had crystallized. The crystals were collected by vacuum filtration, and the moisture on the surface of the crystals was absorbed with dry filter paper.

2.2. Methods

Dehydration Sample Preparations. $ZnSO_4{\cdot}6H_2O$ was obtained after 1 g of fresh $ZnSO_4{\cdot}7H_2O$ lost its 6.3% moisture content on a thermobalance (MB120ZH, OHAUS, Changzhou, China) set at 50 °C. The dehydration sample, mainly composed of $ZnSO_4{\cdot}4H_2O$ ($ZnSO_4{\cdot}4H_2O$*), was obtained by heating 1 g of fresh $ZnSO_4{\cdot}7H_2O$ with 18.9% water lost on a thermobalance set at 70 °C. $ZnSO_4{\cdot}H_2O$ was obtained while 1 g of fresh $ZnSO_4{\cdot}7H_2O$ lost its 37.8% moisture content on a thermobalance set at 150 °C. Anhydrous $ZnSO_4$ was obtained after dehydration treatment for two hours at 350 °C on a hot stage (HP380-Pro, DLAB SCIENTIFIC, Beijing, China) with 1 g of raw $ZnSO_4{\cdot}7H_2O$.

Spray Drying of $ZnSO_4$ Aqueous Solution. A total of 25 $mg{\cdot}mL^{-1}$ $ZnSO_4$ aqueous solution was spray dried (Shanghai Pilotech YC-015, feed rate 1.5–2 $L{\cdot}h^{-1}$, inlet temperature 200 °C, outlet temperature ~110 °C, atomization air pressure 24 $kg{\cdot}cm^{-2}$, drying air flow rate 30 $m^3{\cdot}h^{-1}$).

Conventional Characterization. $ZnSO_4$ samples were characterized with differential scanning calorimetry–thermogravimetric analysis (DSC-TGA, NETZSCH STA 449F3, NETZSCH, Germany, dry N_2, 10 $K{\cdot}min^{-1}$), powder X-ray diffraction (PXRD, Philips X'Pert Pro, PANalytical, Netherlands, Cu Kα, 40 kV, 30 mA, 10–30°, 4°·min^{-1} and Rigaku SmartLab, Cu Kα, 40 kV, 50 mA, 10–30°, 5°·min^{-1}), Fourier transform infrared spectroscopy (IR, Shimadzu IRAffinity-1S, Shimadzu, Japan, absorbance, 400–4000 cm^{-1}) and confocal Raman spectroscopy (Thermo Fisher Scientific, USA, DXR3xi, 532 nm, 40 mW, 0.002–0.02 s, 1000 scans of 50–3400 cm^{-1}, 50× objective lens).

Difference Spectra Analysis. The IR spectrum of $ZnSO_4{\cdot}4H_2O$* is a composite spectrum of the main $ZnSO_4{\cdot}4H_2O$ and a small amount of $ZnSO_4{\cdot}6H_2O$ and $ZnSO_4{\cdot}H_2O$. The

Raman spectrum of $ZnSO_4 \cdot 4H_2O$* is equal to that of $ZnSO_4 \cdot 4H_2O$ because the Raman spectroscopy was obtained from a micro area. The Raman spectrum of $ZnSO_4 \cdot 4H_2O$ in the $ZnSO_4 \cdot 4H_2O$* sample can be easily identified, which is different from that of $ZnSO_4 \cdot 6H_2O$ and $ZnSO_4 \cdot H_2O$. All the obtained spectra were normalized for difference spectra analysis. Briefly, IR bands at 1084 cm^{-1} of $ZnSO_4$ saturated aqueous solution, 1053 cm^{-1} of $ZnSO_4 \cdot 7H_2O$ and $6H_2O$, 1063 cm^{-1} of $ZnSO_4 \cdot 4H_2O$*, 1082 cm^{-1} of $ZnSO_4 \cdot H_2O$, and 1050 cm^{-1} of anhydrous $ZnSO_4$ were used for normalization, and Raman bands at 982 cm^{-1} of aqueous solution and $ZnSO_4 \cdot 6H_2O$, 983 cm^{-1} of $ZnSO_4 \cdot 7H_2O$, 991 cm^{-1} of $ZnSO_4 \cdot 4H_2O$, 1020 cm^{-1} of $ZnSO_4 \cdot H_2O$, and 1040 cm^{-1} of anhydrous $ZnSO_4$ were used for normalization. Difference spectra were obtained by the subtraction of two related spectra with further baseline deduction based on a polynomial fitting method. Absolute deviation of the values in the difference spectrum (*a.d.*) was used to compare the similarity.

$$a.d. = \frac{\sum |x|}{n}$$

Each sample was characterized three times individually, and the corresponding nine difference spectra can be obtained. Further, the error of the *a.d.* can be calculated.

3. Results

3.1. Microscopic DSC-TGA and Macroscopic TGA of $ZnSO_4 \cdot 7H_2O$

Fresh $ZnSO_4 \cdot 7H_2O$ was prepared via slowly evaporating the aqueous solution of $ZnSO_4$. The microscopic TGA curve of fresh $ZnSO_4 \cdot 7H_2O$ with a heating rate of 10 $K \cdot min^{-1}$ reveals a two-stage dehydration process within the temperature range of 25–400 °C (Figure 1a). The first dehydration step takes place below 200 °C with a weight loss of 37.1%, confirmed as the $7 \rightarrow 1$ dehydration process with theoretical weight loss of 37.6%. The second dehydration step occurs in the temperature range of 200–400 °C with a weight loss of 7.6%, similar to the $1 \rightarrow 0$ dehydration process with theoretical weight loss of 6.3%. The microscopic TGA curve does not provide additional insights about the $7 \rightarrow 1$ dehydration process even with a slow heating rate of 1 $K \cdot min^{-1}$ (Figure S1). The corresponding DSC curve exhibits four distinct endothermic peaks at 56, 95, 146, and 315 °C, indicating a four-step dehydration process denoted as $7 \rightarrow X_1 \rightarrow X_2 \rightarrow 1 \rightarrow 0$. X_1 and X_2 are two unknown intermediate phases. The X_1 phase can be obtained because the endothermic peak corresponding to the transition from $7H_2O$ to X_1 is isolated. The synthesis of the X_2 phase with good purity seems to be rather challenging because the endothermic peaks of $X_1 \rightarrow X_2$ and $X_2 \rightarrow 1H_2O$ transformation processes are overlapping even with a slow heating rate of 1 $K \cdot min^{-1}$. The X_2 phase might be unstable and easy to transform into $ZnSO_4 \cdot H_2O$. Macroscopic TGA curves of $ZnSO_4 \cdot 7H_2O$ at different temperatures only show one continuous step in a $7 \rightarrow 1$ process (Figure 1b), similar to the microscopic TGA curves. The weight loss of $ZnSO_4 \cdot 7H_2O$ is 36.0% at 50 °C and 100 °C ($ZnSO_4 + 1.2H_2O$) and 37.8% ($ZnSO_4 + 1.0H_2O$) at 150 °C. The macroscopic TGA curves reach equilibrium within 10 min at 100 and 150 °C, which is too rapid to capture intermediate phases. The macroscopic TGA curve obtained at 50 °C shows a gradual and nearly linear weight loss, which is conducive to obtaining intermediate products with precise compositions (e.g., $ZnSO_4 + 6.0H_2O$, $ZnSO_4 + 4.0H_2O$).

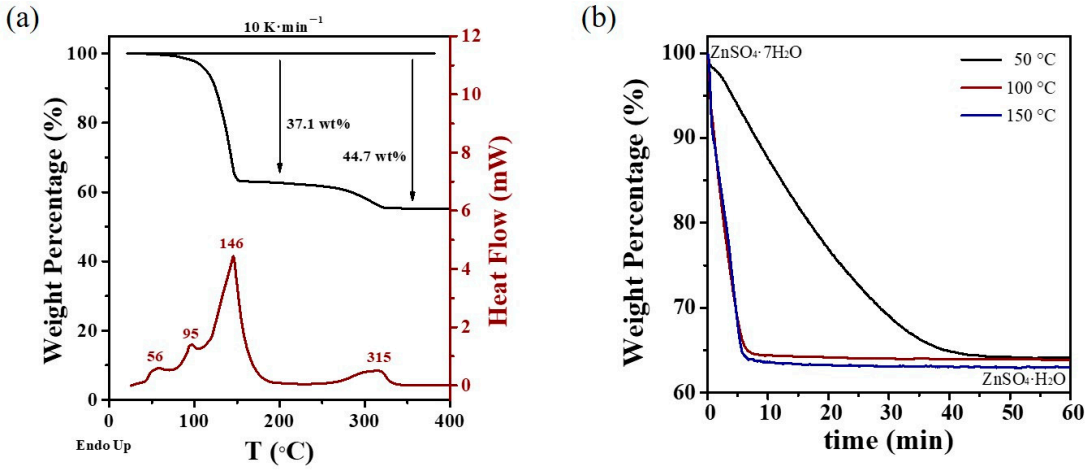


Figure 1. (**a**) Microscopic DSC-TGA curves and (**b**) macroscopic TGA curves at different temperatures (50, 100 and 150 °C) of $ZnSO_4 \cdot 7H_2O$.

3.2. Macroscopic Dehydration Control of $ZnSO_4 \cdot 7H_2O$

Four phases, including $ZnSO_4 \cdot 7H_2O$, $ZnSO_4 \cdot 6H_2O$, $ZnSO_4 \cdot H_2O$ and anhydrous $ZnSO_4$, can be prepared with good purity and robust repeatability via macroscopic TGA, confirmed by the simulated PXRD patterns of the pure phases. The characteristic 2θ peaks of $ZnSO_4$ hydrates are compared and identified (Table S1). The fresh $ZnSO_4 \cdot 7H_2O$ is confirmed again from the PXRD pattern (Figure 2a). The sample of $ZnSO_4 + 6.0H_2O$ is the product of fresh $ZnSO_4 \cdot 7H_2O$ with 6.3% weight loss in the macroscopic TGA carried out at 50 °C, whose PXRD pattern aligns with the simulated PXRD pattern of $ZnSO_4 \cdot 6H_2O$ (Figure 2b). $ZnSO_4 + 1.0H_2O$ is the equilibrium product of $ZnSO_4 \cdot 7H_2O$ in the macroscopic TGA carried out at 150 °C, and its PXRD pattern agrees with the simulated PXRD pattern of $ZnSO_4 \cdot H_2O$ (Figure 2c). The equilibrium product of $ZnSO_4 \cdot 7H_2O$ in the macroscopic TGA at 50 °C is $ZnSO_4 + 1.2H_2O$, and its PXRD pattern is also consistent with that of $ZnSO_4 \cdot H_2O$. The water content of $ZnSO_4 \cdot H_2O$ can be variable. Anhydrous $ZnSO_4$ is the equilibrium product of the macroscopic TGA at 350 °C confirmed by the PXRD pattern (Figure 2d). After being stored in a sealed environment for one week, the PXRD patterns of these four phases remained unchanged, indicating good storage stability. Through macroscopic TGA, the exact water contents of $ZnSO_4 \cdot 6H_2O$ and $ZnSO_4 \cdot H_2O$ can be precisely determined and controlled, which is an advantage that other methods do not possess.

$ZnSO_4$ samples with precise water contents of $5.0H_2O$, $4.0H_2O$, $3.0H_2O$ and $2.0H_2O$ can be easily prepared by macroscopic TGA at 50 °C. After a careful comparison, we found that the PXRD patterns of these fresh samples only show the characteristic 2θ peaks of $ZnSO_4 \cdot 6H_2O$ and $ZnSO_4 \cdot H_2O$ (Figure 3a). The characteristic 2θ peaks of $ZnSO_4 \cdot 4H_2O$ at 13.0, 22.5, 24.8, 27.4° are all not observed. The diffraction intensity ratio of the peak at 20.3° of $ZnSO_4 \cdot 6H_2O$ and peak at 26.2° of $ZnSO_4 \cdot H_2O$ shows a good linear relationship with the mass ratio of $ZnSO_4 \cdot 6H_2O$ and $ZnSO_4 \cdot H_2O$ (Figure S2), indirectly confirming that these samples only contain $ZnSO_4 \cdot 6H_2O$ and $ZnSO_4 \cdot H_2O$. $ZnSO_4 \cdot 4H_2O$ is a distinct kinetic intermediate phase, which can only be obtained under a suitable dehydration rate. The $ZnSO_4 + 4.0H_2O$ sample can also be easily prepared by conducting macroscopic TGA at a higher temperature (Figure 3b). When the operation temperature was 60 °C, a small amount of $ZnSO_4 \cdot 4H_2O$ appeared. $ZnSO_4 \cdot 4H_2O$ became the main product when macroscopic TGA was carried out at 70–80 °C. The proportion of $ZnSO_4 \cdot 4H_2O$ declined at the operation temperature of 90 °C. The $ZnSO_4 + 4.0H_2O$ obtained at 70 °C ($ZnSO_4 \cdot 4H_2O$*) was selected to study the physical and chemical properties of $ZnSO_4 \cdot 4H_2O$ due to its high content of $ZnSO_4 \cdot 4H_2O$ and the low operation temperature. By carefully compar-

ing the PXRD patterns, it can be concluded that $ZnSO_4 \cdot 4H_2O$* is a mixture of primary $ZnSO_4 \cdot 4H_2O$, $ZnSO_4 \cdot 6H_2O$ and $ZnSO_4 \cdot H_2O$. The composition of $ZnSO_4$ + 5.0H_2O obtained at 70 °C is mainly $ZnSO_4 \cdot 6H_2O$ with a small amount of $ZnSO_4 \cdot 4H_2O$ (Figure 3c). The $ZnSO_4$ + 4.0H_2O obtained from $ZnSO_4 \cdot 6H_2O$ at 70 °C is also mainly composed of $ZnSO_4 \cdot 4H_2O$, similar to $ZnSO_4 \cdot 4H_2O$*. The direct transformation from $ZnSO_4 \cdot 7H_2O$ to $ZnSO_4 \cdot 4H_2O$ was not observed. $ZnSO_4 \cdot 4H_2O$ was mainly formed by the dehydration of $ZnSO_4 \cdot 6H_2O$. Thus, we consider that for the $7 \rightarrow X_1 \rightarrow X_2 \rightarrow 1 \rightarrow 0$ dehydration process indicated by microscopic DSC-TGA mentioned above, X_1 is $ZnSO_4 \cdot 6H_2O$ and X_2 is $ZnSO_4 \cdot 4H_2O$. The gradual dehydration process of $ZnSO_4 \cdot 7H_2O$ can be $7 \rightarrow 6 \rightarrow 4 \rightarrow 1$ and $7 \rightarrow 6 \rightarrow 1$ in this work. $ZnSO_4 \cdot 4H_2O$* was not stable and would transform into a product composed of $ZnSO_4 \cdot 6H_2O$ (main) and $ZnSO_4 \cdot H_2O$ even after only one day of storage (Figure 3d). $ZnSO_4 \cdot 4H_2O$ was hardly detectable in the PXRD pattern after storage for 5 days. $ZnSO_4 \cdot 4H_2O$* should be characterized as soon as possible to avoid its polymorphism transition.

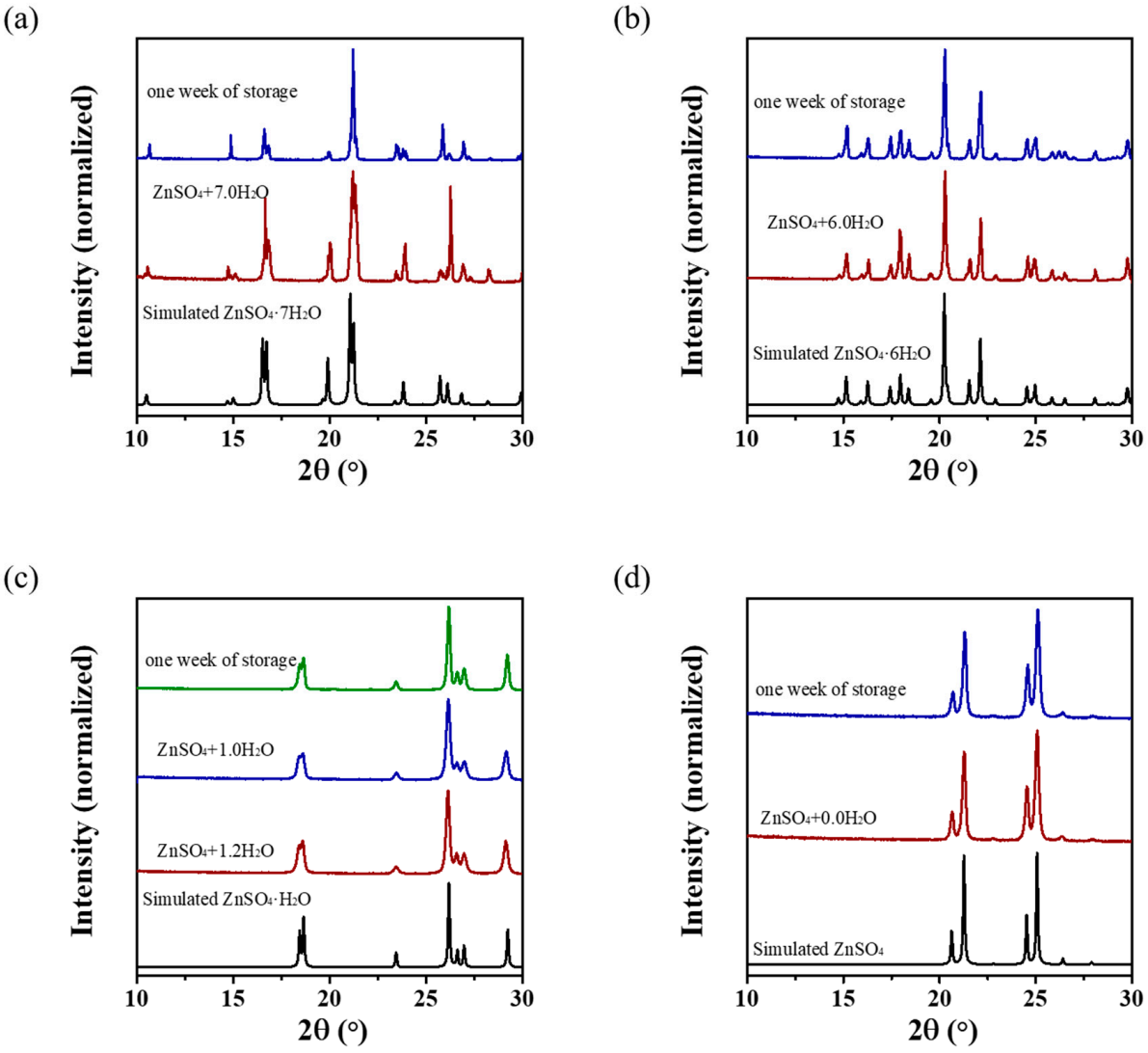


Figure 2. Preparations of $ZnSO_4 \cdot 7H_2O$, $ZnSO_4 \cdot 6H_2O$, $ZnSO_4 \cdot H_2O$ and anhydrous $ZnSO_4$ with high purity. PXRD patterns of fresh and stored (**a**) $ZnSO_4$ + 7.0H_2O (freshly obtained by slow evaporation of ZnSO4 aqueous solution, (**b**) $ZnSO_4$ + 6.0H_2O (obtained with macroscopic TGA at 50 °C), (**c**) $ZnSO_4$ + 1.0H_2O obtained with macroscopic TGA carried out at 150 °C and $ZnSO_4$ + 1.2H_2O obtained with macroscopic TGA at 50 °C, and (**d**) $ZnSO_4$ + 0.0H_2O prepared by macroscopic TGA at 350 °C. The PXRD pattern simulation was carried out with Mercury 2022.3.0 software.

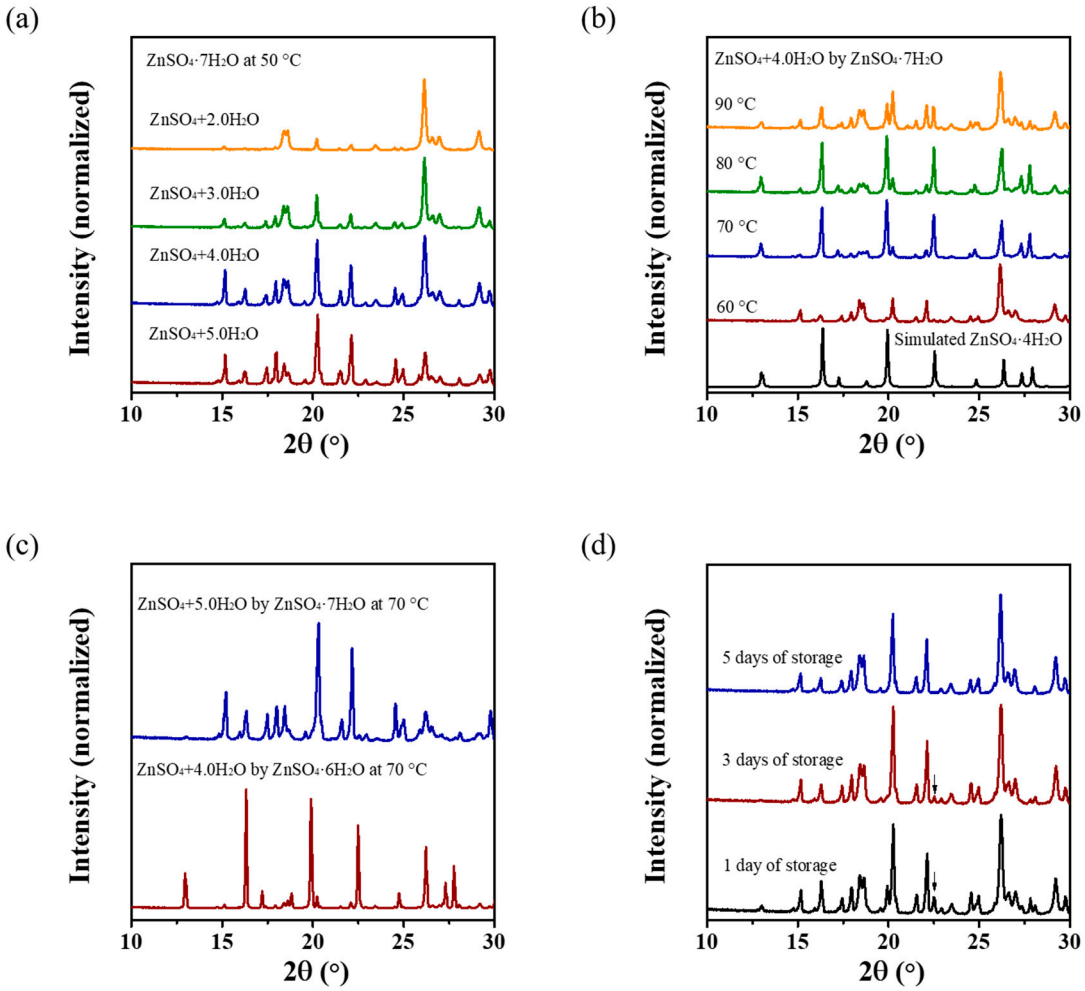


Figure 3. Preparations of $ZnSO_4 \cdot 4H_2O$ as the main product. PXRD patterns of (**a**) $ZnSO_4$ + 5.0H_2O, 4.0H_2O, 3.0H_2O and 2.0H_2O prepared from $ZnSO_4 \cdot 7H_2O$ in the macroscopic TGA carried out at 50 °C, (**b**) $ZnSO_4$ + 4.0H_2O obtained at 60, 70 ($ZnSO_4 \cdot 4H_2O$*), 80 and 90 °C, (**c**) $ZnSO_4$ + 4.0H_2O prepared from $ZnSO_4 \cdot 6H_2O$ via macroscopic TGA carried out at 70 °C, (**d**) $ZnSO_4 \cdot 4H_2O$* after being stored for 1, 3, 5 days (the characteristic peak of $ZnSO_4 \cdot 4H_2O$ marked with a black arrow disappeared after being stored for 5 days).

3.3. Vibrational Spectroscopic Analysis

The spectroscopic method has been widely used in the field of hydrates [37]. Spectroscopic techniques are usually non-destructive, and can provide information at the molecular levels, which is helpful for understanding the dehydration process. The limitation of the spectroscopic method lies in the fact that without the PXRD results or standard spectra, the crystal form cannot be determined. The combination of macroscopic TGA and PXRD makes it possible to study the dehydration of $ZnSO_4 \cdot 7H_2O$ by infrared (IR) and Raman spectroscopy.

Mid-frequency IR spectra (in the range of 400–1800 cm^{-1}, Figure 4a, Table 3) show the main signals of $ZnSO_4$ samples, while high-frequency IR spectra do not provide much information (Figure S3). The IR spectrum of $ZnSO_4$ saturated aqueous solution shows two strong bands at 1084 cm^{-1} (ν_3-SO_4^{2-}, asymmetric stretching vibration band) and 1643 cm^{-1} (δ-OH), and two weak bands at 601 cm^{-1} (δ_{as}-SO_4^{2-}, asymmetrical angular vibration band) and 980 cm^{-1} (ν_1-SO_4^{2-}, symmetric stretching vibration band) [17,38]. ν_3 at 1053 cm^{-1} is observed in $ZnSO_4 \cdot 7H_2O$ and $ZnSO_4 \cdot 6H_2O$, and shifts to 1063 cm^{-1} for $ZnSO_4 \cdot 4H_2O$* and 1082 cm^{-1} for $ZnSO_4 \cdot H_2O$. δ-OH exists in $ZnSO_4 \cdot 7H_2O$, $6H_2O$ and $4H_2O$*, and disappears in $ZnSO_4 \cdot H_2O$ and anhydrous $ZnSO_4$. The IR spectrum of anhydrous $ZnSO_4$ is quite

different from those of the other samples, indicating a different molecular packing pattern. IR difference spectra analysis was used to establish the similarity orders among $ZnSO_4$ samples, as reported in our previous work [39]. The absolute deviations of values in the IR difference spectra show that the similarity can be easily divided into three regions (Figure 4b). The most similar region is 7–6. The second similar region includes aq-7, aq-6, aq-4,7-4, 6-4, and 4-1. The other comparisons show poor similarities.

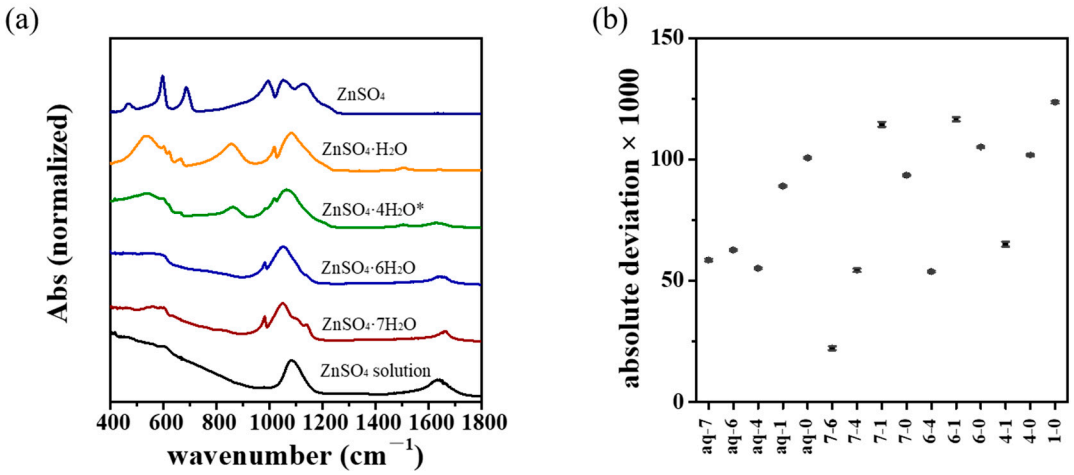


Figure 4. Mid-frequency IR spectroscopic analysis among $ZnSO_4$ solution (aq), $ZnSO_4{\cdot}7H_2O$, $ZnSO_4{\cdot}6H_2O$, $ZnSO_4{\cdot}4H_2O$*, $ZnSO_4{\cdot}H_2O$ and anhydrous $ZnSO_4$. (**a**) IR spectra and (**b**) absolute deviation (*a.d.*) of values in the IR difference spectra in the range of 400–1800 cm^{-1}. The errors of the *a.d.* are shown.

Table 3. Mid-frequency IR bands of $ZnSO_4$ samples.

Solution	$7H_2O$	$6H_2O$	$4H_2O$*	$1H_2O$	Anhydrous	Assignment [38]
					470	
	561	557	536	534		
601	602	597	600	601	599	δ_{as}-SO_4^{2-}
				623		
			665	665	689	
			861	855		
980	982	982	984		992	ν_1-SO_4^{2-}
			1017	1017		
	1053	1053	1063		1050	
1084				1082		ν_3-SO_4^{2-}
	1142				1129	
			1504	1504		
1643	1661	1651	1632			δ-OH

Low-frequency Raman spectroscopy (LFRS, below 300 cm^{-1}) is associated with lattice vibrations, which is often used to distinguish polymorphs [40,41]. The LFRS of $ZnSO_4$ aqueous solution does not show obvious bands, confirming the features of the solution. The LFRS values of $ZnSO_4{\cdot}7H_2O$ (59, 69, 107, 127, 193, 220, 238 cm^{-1}), $ZnSO_4{\cdot}6H_2O$ (66, 96, 111, 133, 221, 236 cm^{-1}), $ZnSO_4{\cdot}4H_2O$ (52, 78, 102, 126, 149, 178, 221, 277 cm^{-1}), $ZnSO_4{\cdot}H_2O$ (112, 171, 218, 278 cm^{-1}) and anhydrous $ZnSO_4$ (95, 139, 184 cm^{-1} with a poor signal-to-noise ratio) show different characteristic Raman bands (Figure 5).

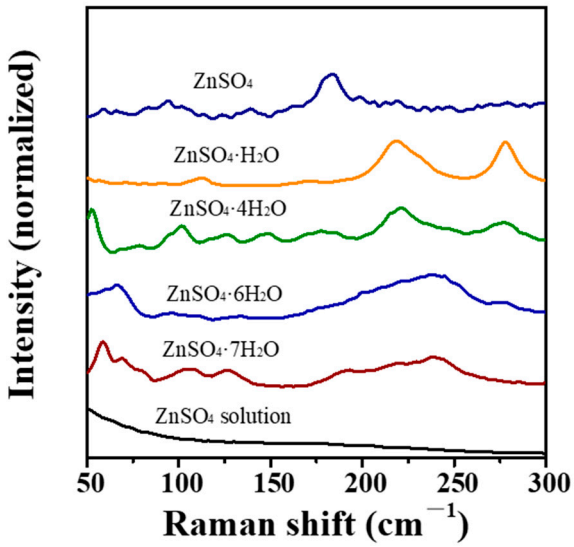


Figure 5. Low-frequency Raman spectra of $ZnSO_4$ samples.

Mid-frequency Raman spectra (MFRS, range of 300–1800 cm^{-1}, Figure 6a, Table 4) showing the molecular vibration signals with a good signal-to-noise ratio are commonly used for compound identification [42], whereas high-frequency Raman spectra do not provide useful information (Figure S4). The MFRS of $ZnSO_4$ solution shows one strong band at 982 cm^{-1} (ν_1-SO_4^{2-}), and three weak bands at 448, 613, and 1104 cm^{-1}, corresponding to ν_2-SO_4^{2-} (depolarized deformation modes), ν_4-SO_4^{2-} (depolarized deformation modes), and ν_3-SO_4^{2-} [43,44]. The MFRS values of $ZnSO_4$ solution, $ZnSO_4{\cdot}7H_2O$, $6H_2O$, $4H_2O$ and $1H_2O$ are similar in visual. The strong ν_1 of $ZnSO_4$ solution, $ZnSO_4{\cdot}7H_2O$ and $6H_2O$ is at 982 cm^{-1}, and shifts to 991 cm^{-1} for $4H_2O$ and 1020 cm^{-1} for $1H_2O$. The MFRS of anhydrous $ZnSO_4$ is different from those of the other $ZnSO_4$ samples. Mid-frequency Raman difference spectra analysis was also used to establish the similarity orders [39] among $ZnSO_4$ samples. The absolute deviations of the values in Raman difference spectra show that the similarity can be divided into four regions (Figure 6b). The most similar region is aq-7, aq-6, and 7-6. The second similar region includes aq-4, 7-4, and 6-4. The third similar region includes aq-1, 7-1, and 6-1. The comparison of 4-1 is between the second region and the third region. The other comparisons show poor similarities.

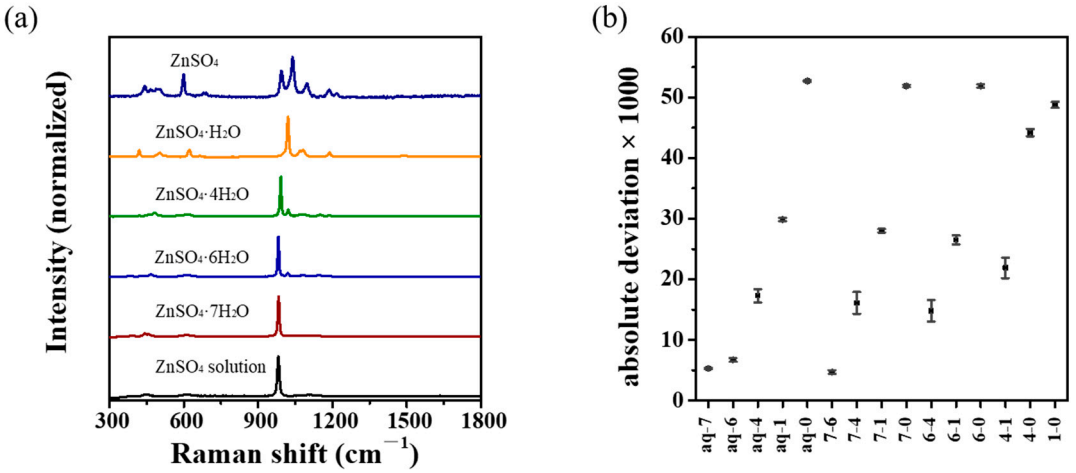


Figure 6. Mid-frequency Raman spectra (in the range of 300–1800 cm^{-1}) analysis of $ZnSO_4$ samples. (**a**) Raman spectra and (**b**) absolute deviation (*a.d.*) of values in the Raman difference spectra. The errors of the *a.d.* are shown.

Table 4. Mid-frequency Raman bands of $ZnSO_4$ samples.

Solution	$7H_2O$	$6H_2O$	$4H_2O$	$1H_2O$	Anhydrous	Assignment [43,44]
448	442		421	420	442	ν_2-SO_4^{2-}
		466	483		468	
				503	496	
613	612	619	624	623	600	ν_4-SO_4^{2-}
					691	
982	983	982	991		993	ν_1-SO_4^{2-}
		1020	1022	1020	1040	
	1058		1073	1071		
1104	1094	1080		1082	1098	ν_3-SO_4^{2-}
	1140	1144	1151			
			1188	1188	1186	
					1218	

3.4. Crystallographic Analysis

The crystal structure of $ZnSO_4{\cdot}7H_2O$ (Figure 7a) reveals the presence of two distinct zinc ions in the unit cell. The coordination environments of the two Zn^{2+} are identical, coordinated with six water molecules in the form of $[Zn(H_2O)_6]^{2+}$, but the orientations of the two $[Zn(H_2O)_6]^{2+}$ are different. SO_4^{2-} does not coordinate with Zn^{2+}. $ZnSO_4{\cdot}7H_2O$ can be represented as $[Zn(H_2O)_6]SO_4{\cdot}H_2O$. The two O atoms in the sulfate group are connected to the water molecule of two $[Zn(H_2O)_6]^{2+}$ molecules with hydrogen bonding, forming a zigzag one-dimensional chain structure denoted as $[Zn(H_2O)_6SO_4]_n$. The additional water molecule is linked to $[Zn(H_2O)_6]^{2+}$ and SO_4^{2-} with hydrogen bonding. Although the crystal structure of $ZnSO_4{\cdot}6H_2O$ (Figure 7b) is different from that of $ZnSO_4{\cdot}7H_2O$, the coordination environments of Zn^{2+} and SO_4^{2-} in $ZnSO_4{\cdot}6H_2O$ are almost the same as those in $ZnSO_4{\cdot}7H_2O$, which can be represented as $[Zn(H_2O)_6]SO_4$. The unit cell of $ZnSO_4{\cdot}6H_2O$ contains two $[Zn(H_2O)_6]^{2+}$ molecules with different orientations. The crystal structure of $ZnSO_4{\cdot}4H_2O$ (Figure 7c) reveals that the coordination environment of Zn^{2+} is $[Zn(H_2O)_4(1/2SO_4)_2]$ with two orientations. The two O atoms of SO_4^{2-} are coordinated with a Zn^{2+} ion. The crystal structure of $ZnSO_4{\cdot}H_2O$ (Figure 7d) reveals that the coordination environment of Zn^{2+} changes $[Zn(1/2H_2O)_2(1/4SO_4)_4]$, the O atom of water is coordinated with two Zn^{2+} ions and each O atom of SO_4^{2-} is coordinated with one Zn^{2+} ion. The crystal structure of anhydrous $ZnSO_4$ (Figure 7e) has a high degree of symmetry compared to $ZnSO_4$ hydrates. The coordination environment of Zn^{2+} can be written as $[Zn(1/4SO_4)_4]$ which is different from the hexacoordinated Zn^{2+}, and the coordination environment of SO_4^{2-} is similar to that in $ZnSO_4{\cdot}H_2O$. The significant differences of the Zn^{2+} coordination environment between $ZnSO_4{\cdot}H_2O$ and anhydrous $ZnSO_4$ make the direct transformation between them difficult, which can explain the appearance of a liquid intermediate phase [45].

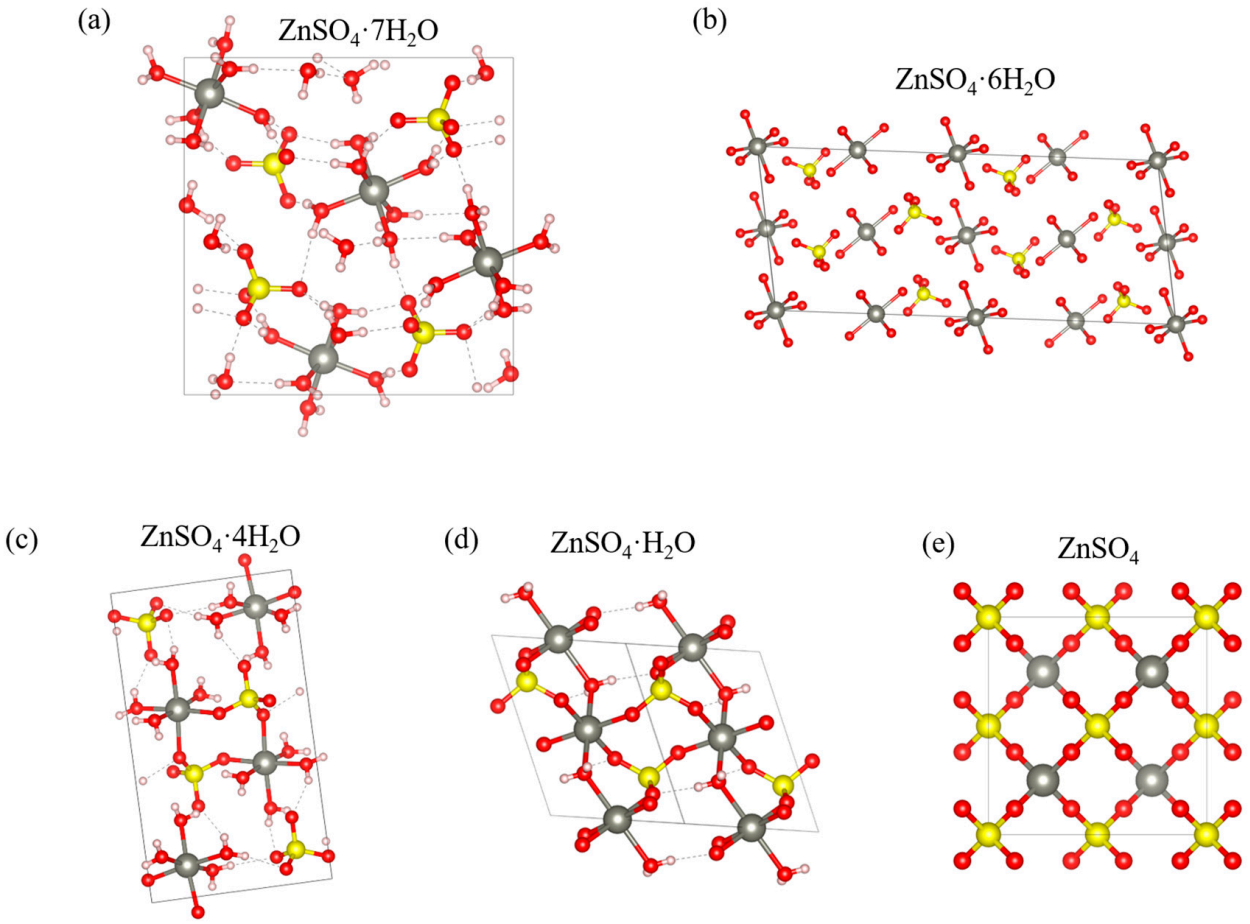


Figure 7. Crystal structure analysis among (**a**) $ZnSO_4·7H_2O$, (**b**) $ZnSO_4·6H_2O$, (**c**) $ZnSO_4·4H_2O$, (**d**) $ZnSO_4·H_2O$ and (**e**) anhydrous $ZnSO_4$ (gray: Zn, yellow: S, red: O, white: H).

3.5. Similarity Analysis

Similarity analysis based on different methods may yield different results. It is necessary to adopt various methods to perform the structural similarity analysis. Herein, vibrational spectroscopy and crystal structure are used to determine the similarity order. IR difference spectra indicate that $7H_2O$ and $6H_2O$ are most similar, suggesting a kinetic dehydration process of $7 \rightarrow 6$. $4H_2O$ is the most similar to $6H_2O$ in the dehydration process of $6H_2O$, suggesting a kinetic process of $6 \rightarrow 4$. The kinetic process of $4 \rightarrow 1$ is proposed with similar analysis. The IR spectra analysis suggests that the gradual dehydration process of $7H_2O$ is $7 \rightarrow 6 \rightarrow 4 \rightarrow 1 \rightarrow 0$ (Figure 8a). Raman difference spectra analysis shows similar results to IR difference spectra analysis, except in the dehydration process of $6H_2O$; the kinetic process can be $6 \rightarrow 4$ or $6 \rightarrow 1$. The Raman spectra analysis suggests that the gradual dehydration process of $7H_2O$ is $7 \rightarrow 6 \rightarrow 4 \rightarrow 1 \rightarrow 0$ and $7 \rightarrow 6 \rightarrow 1 \rightarrow 0$ (Figure 8b). The simplified coordination environments of Zn^{2+} in various crystal structures are schematized and compared (Figure 8c). The simplified Zn^{2+} environments are $[Zn(H_2O)_6]^{2+}$ in $7H_2O$ and $6H_2O$, $[Zn(H_2O)_4(1/2SO_4)_2]$ in $4H_2O$, $[Zn(1/2H_2O)_2(1/4SO_4)_4]$ in $1H_2O$, and $[Zn(1/4SO_4)_4]$ in anhydrous $ZnSO_4$. The coordination environment analysis of Zn^{2+} suggests that the gradual dehydration process of $7H_2O$ is $7 \rightarrow 6 \rightarrow 4 \rightarrow 1 \rightarrow 0$. The simplified coordination environment of SO_4^{2-} suggests that the gradual dehydration process of $7H_2O$ is $7 \rightarrow 6 \rightarrow 4 \rightarrow 1 \rightarrow 0$ and $7 \rightarrow 6 \rightarrow 4 \rightarrow 0$ (Figure 8d). Both the similarity analysis based on vibrational spectroscopy and crystal structure suggest that the kinetic gradual dehydration process of $ZnSO_4·7H_2O$ is $7 \rightarrow 6 \rightarrow 4 \rightarrow 1 \rightarrow 0$.

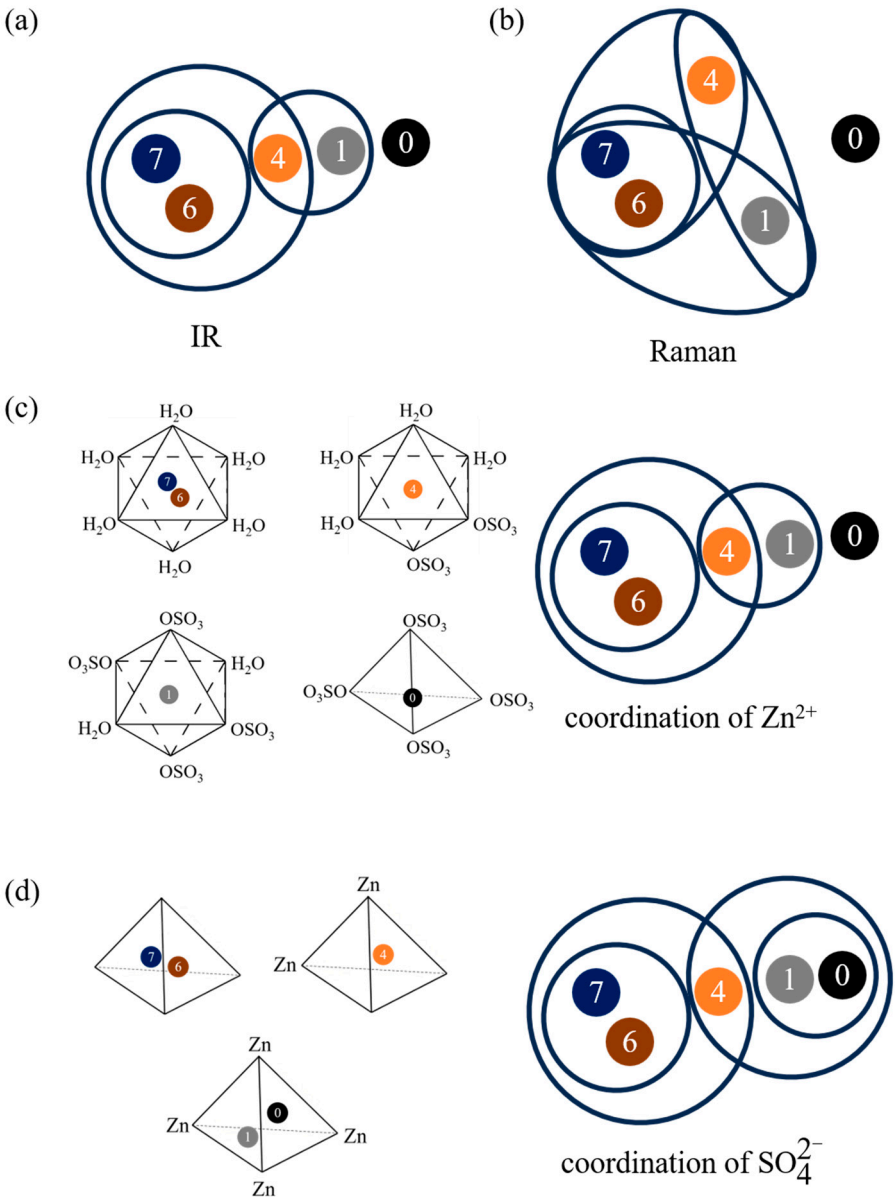


Figure 8. Structural similarity analysis based on (**a**) IR spectra, (**b**) Raman spectra, and coordination environment of (**c**) Zn^{2+} and (**d**) SO_4^{2-} among $ZnSO_4{\cdot}7H_2O$, $ZnSO_4{\cdot}6H_2O$, $ZnSO_4{\cdot}4H_2O$, $ZnSO_4{\cdot}H_2O$ and anhydrous $ZnSO_4$. $ZnSO_4{\cdot}nH_2O$ is represented by the number of water molecules (7, 6, 4, 1 and 0) it contains.

4. Discussion

4.1. Macroscopic TGA Combined with PXRD

Macroscopic TGA and PXRD are very common methods in the laboratory and industry. The combination of macroscopic TGA and PXRD is a feasible method that enables the acquisition of intermediate products with precise water content and accurate polymorph during the dehydration process of hydrates. Macroscopic TGA ensures the precise determination of compositions, while PXRD guarantees the accurate identification of crystalline forms. Macroscopic TGA conducted under different conditions may induce different dehydration processes and result in different products. Products with precise compositions and accurate polymorphs are conducive to obtaining the fundamental spectra, which is difficult to achieve through other methods. Acquisition of these fundamental data facilitates the proposal of dehydration mechanisms and designs of the thermal energy storage and release systems based on $ZnSO_4{\cdot}7H_2O$ [46]. The method combining macroscopic TGA with PXRD

is also suitable for capturing the intermediate phases during the desolvation process of solvates and the solvent evaporation crystallization process.

4.2. Preparations of $ZnSO_4 \cdot 4H_2O$

$ZnSO_4 \cdot 4H_2O$ single crystal can be prepared via vapor phase diffusion of diethyl ether into a reflux acetonitrile solution of hydrated zinc tetrafluoroborate and 2,6-bis(2-mercapto-1-methylimidazole)pyridine after a period of seven months [47], showing that it is difficult to prepare $ZnSO_4 \cdot 4H_2O$. Based on the results of similarity analysis, it is possible to obtain $ZnSO_4 \cdot 4H_2O$ at room temperature with a suitable humidity through the $7 \rightarrow 6 \rightarrow 4$ dehydration process. The PXRD patterns indicate that under atmospheric conditions (26 °C, 60% humidity), $ZnSO_4 \cdot 7H_2O$ mainly transforms into $ZnSO_4 \cdot 6H_2O$ after 3 days and into $ZnSO_4 \cdot 4H_2O$ with a small amount of $ZnSO_4 \cdot H_2O$ after 5 days (Figure 9a). The sample mainly composed of $ZnSO_4 \cdot 4H_2O$ remained stable even after being exposed to the air for one month. IR and Raman spectroscopic analyses also indicate that it is possible to crystalize $ZnSO_4 \cdot 4H_2O$ from $ZnSO_4$ aqueous solution. The spray drying product of $ZnSO_4$ aqueous solution is a mixture of $ZnSO_4 \cdot 4H_2O$ and $ZnSO_4 \cdot H_2O$ (Figure 9b). Similarity principle can guide the preparation methods of metastable intermediate phases. However, neither of these two methods can prepare pure phase of $ZnSO_4 \cdot 4H_2O$ with accurate composition. The macroscopic dehydration of $ZnSO_4 \cdot 7H_2O$ at 70 °C to $ZnSO_4 + 4.0H_2O$ is a quick and feasible method for the preparation of $ZnSO_4 \cdot 4H_2O$.

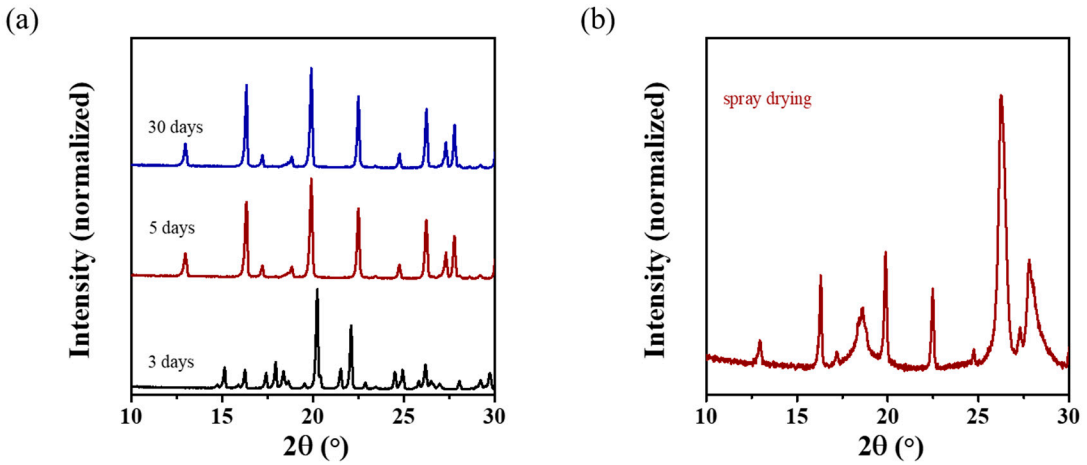


Figure 9. Preparations of $ZnSO_4 \cdot 4H_2O$. PXRD patterns of (**a**) dehydration products of $ZnSO_4 \cdot 7H_2O$ under air (26 °C, 60% humidity) after 3, 5, and 30 days, (**b**) spray drying product of $ZnSO_4$ aqueous solution.

5. Conclusions

In the dehydration process of $ZnSO_4 \cdot 7H_2O$, intermediate hydrates with precise water contents, including $ZnSO_4 \cdot 6H_2O$, $ZnSO_4 \cdot 4H_2O$ and $ZnSO_4 \cdot H_2O$, were prepared by macroscopic TGA and confirmed by PXRD. IR and Raman spectra of the various $ZnSO_4$ hydrates were obtained and compared for the first time. IR, Raman spectroscopic analysis and crystallographic analysis explain the gradual dehydration process of $7 \rightarrow 6 \rightarrow 4 \rightarrow 1 \rightarrow 0$ based on the principle of similarity. Macroscopic TGA combined with PXRD is a feasible method for preparing intermediate hydrates with precise water contents and accurate polymorphs, and obtaining the related spectra in the dehydration process of hydrates.

Supplementary Materials: The following supporting information can be downloaded at: https://www.mdpi.com/article/10.3390/cryst15030257/s1, Table S1: Characteristic 2θ peaks of $ZnSO_4 \cdot nH_2O$; Figure S1: DSC-TGA curve of $ZnSO_4 \cdot 7H_2O$ with a heating rate of 1 $K \cdot min^{-1}$; Figure S2:

Linear relationship between the PXRD diffraction intensity ratio and the mass ratio of $ZnSO_4 \cdot 6H_2O$ and $ZnSO_4 \cdot H_2O$; Figure S3: High-frequency IR spectra of $ZnSO_4$ samples; Figure S4: High-frequency Raman spectra of $ZnSO_4$ samples.

Author Contributions: Conceptualization, methodology, supervision, resources, F.C. and R.X.; project administration, investigation, data curation, validation, C.D. and W.Z.; visualization, writing—original draft preparation, F.C.; writing—review and editing, R.X.; funding acquisition, F.C. and R.X. All authors have read and agreed to the published version of the manuscript.

Funding: This research was funded by the National Natural Science Foundation of China (grant number 22005175), the Natural Science Foundation of Fujian Province (grant number 2020J01374, 2021J011116).

Data Availability Statement: The original contributions presented in the study are included in the article/Supplementary Material; further inquiries can be directed to the corresponding authors.

Conflicts of Interest: The authors declare no conflicts of interest.

References

1. Makatun, V.N.; Shchegrov, L.N. State of water in inorganic crystal hydrates and the characteristic features of their dehydration. *Russ. Chem. Rev.* **1972**, *41*, 905. [CrossRef]
2. Li, Y.; Li, C.; Lin, N.; Xie, B.; Zhang, D.; Chen, J. Review on tailored phase change behavior of hydrated salt as phase change materials for energy storage. *Mater. Today Energy* **2021**, *22*, 100866. [CrossRef]
3. Hua, W.; Yan, H.; Zhang, X.; Xu, X.; Zhang, L.; Shi, Y. Review of salt hydrates-based thermochemical adsorption thermal storage technologies. *J. Energy Storage* **2022**, *56*, 106158. [CrossRef]
4. Yan, T.S.; Li, T.X.; Xu, J.X.; Chao, J.W. Understanding the transition process of phase change and dehydration reaction of salt hydrate for thermal energy storage. *Appl. Therm. Eng.* **2020**, *166*, 114655. [CrossRef]
5. Xu, J.; Li, T.; Yan, T.; Chao, J.; Wang, R. Dehydration kinetics and thermodynamics of magnesium chloride hexahydrate for thermal energy storage. *Sol. Energy Mater. Sol. Cells* **2021**, *219*, 110819. [CrossRef]
6. Okhrimenko, L.; Dussouillez, J.; Johannes, K.; Kuznik, F. Thermodynamic equilibrium and kinetic study of lanthanum chloride heptahydrate dehydration for thermal energy storage. *J. Energy Storage* **2022**, *48*, 103562. [CrossRef]
7. Xie, N.; Huang, Z.; Luo, Z.; Gao, X.; Fang, Y.; Zhang, Z. Inorganic salt hydrate for thermal energy storage. *Appl. Sci.* **2017**, *7*, 1317. [CrossRef]
8. Man, X.; Lu, H.; Xu, Q.; Wang, C.; Ling, Z. Review on the thermal property enhancement of inorganic salt hydrate phase change materials. *J. Energy Storage* **2023**, *72*, 108699. [CrossRef]
9. Raijada, D.; Arnfast, L.; Bond, A.D.; Aho, J.; Bøtker, J.; Sandler, N.; Rantanen, J. Dehydration of nitrofurantoin monohydrate during melt extrusion. *Cryst. Growth Des.* **2017**, *17*, 3707–3715. [CrossRef]
10. Preturlan, J.G.D.; Vieille, L.; Quiligotti, S.; Favergeon, L. Kinetics and mechanism of the dehydration of calcium sulfate dihydrate: A comprehensive approach for studying the dehydration of ionic hydrates under controlled temperature and water vapor pressure. *J. Phys. Chem. C* **2020**, *124*, 26352–26367. [CrossRef]
11. Eaby, A.C.; Myburgh, D.C.; Kosimov, A.; Kwit, M.; Esterhuysen, C.; Janiak, A.M.; Barbour, L.J. Dehydration of a crystal hydrate at subglacial temperatures. *Nature* **2023**, *616*, 288–292. [CrossRef]
12. Koplík, J.; Švec, J.; Másilko, J.; Sedlačík, M.; Bartoníčková, E. Synthesis of calcium aluminate hydrates, their characterization and dehydration. *Ceram. Int.* **2025**, *51*, 5536–5543. [CrossRef]
13. de Castelnuovo, S.; Harness, J.B.; McColm, I.J. The role of liquid water in crystalline hydrate dehydration: Copper sulphate pentahydrate. *J. Therm. Anal. Calorim.* **2001**, *63*, 233–247. [CrossRef]
14. Cheng, L.; Li, W.; Li, Y.; Yang, Y.; Li, Y.; Cheng, Y.; Song, D. Thermal analysis and decomposition kinetics of the dehydration of copper sulfate pentahydrate. *J. Therm. Anal. Calorim.* **2019**, *135*, 2697–2703. [CrossRef]
15. Gamo, I. Infrared absorption spectra of water of crystallization in copper sulfate penta- and monohydrate crystals. *Bull. Chem. Soc. Jpn.* **1961**, *34*, 764–766. [CrossRef]
16. White, R.L. Variable temperature infrared study of copper sulfate pentahydrate dehydration. *Thermochim. Acta* **2012**, *528*, 58–62. [CrossRef]
17. Widjaja, E.; Chong, H.H.; Tjahjono, M. Use of thermo-Raman spectroscopy and chemometric analysis to identify dehydration steps of hydrated inorganic samples—Application to copper sulfate pentahydrate. *J. Raman Spectrosc.* **2010**, *41*, 181–186. [CrossRef]
18. Rabbering, G.; Wanrooy, J.; Schuijff, A. The dehydration of $ZnSO_4 \cdot 7H_2O$ and $NiSO_4 \cdot 6H_2O$. *Thermochim. Acta* **1975**, *12*, 57–63. [CrossRef]

19. Anderson, J.L.; Peterson, R.C.; Swainson, I.P. Combined neutron powder and X-ray single-crystal diffraction refinement of the atomic structure and hydrogen bonding of goslarite ($ZnSO_4 \cdot 7H_2O$). *Mineral. Mag.* **2005**, *69*, 259–271. [CrossRef]
20. Anderson, J.L.; Peterson, R.C.; Swainson, I.P. The atomic structure of deuterated boyleite $ZnSO_4 \cdot 4D_2O$, ilesite $MnSO_4 \cdot 4D_2O$, and bianchite $ZnSO_4 \cdot 6D_2O$. *Am. Mineral.* **2012**, *97*, 1905–1914. [CrossRef]
21. Chihara, H.; Seki, S. Studies of crystalline hydrates. II. Thermal transition and dehydration of Ni-, Fe-, Co-, Zn-, Mn-, and Mg-sulfate hydrates. *Bull. Chem. Soc. Jpn.* **1953**, *26*, 88–92. [CrossRef]
22. Wheeler, R.C.; Frost, G.B. A comparative study of the dehydration kinetics of several hydrated salts. *Can. J. Chem.* **1955**, *33*, 546–561. [CrossRef]
23. Razouk, R.I.; Mikhail, R.S.; Ghorab, H.Y. Dehydration and rehydration behaviour of zinc and magnesium sulphate heptahydrates. *J. Appl. Chem.* **1969**, *19*, 329–335. [CrossRef]
24. Grønvold, F.; Meisingset, K.K. Thermodynamic properties and phase transitions of salt hydrates between 270 and 400 K I. $NH4Al(SO_4)_2 \cdot 12H_2O$, $KAl(SO_4)_2 \cdot 12H_2O$, $Al_2(SO_4)_3 \cdot 17H_2O$, $ZnSO_4 \cdot 7H_2O$, $Na_2SO_4 \cdot 10H_2O$, and $Na_2S_2O_3 \cdot 5H_2O$. *J. Chem. Thermodyn.* **1982**, *14*, 1083–1098. [CrossRef]
25. Straszko, J.; Olszak-Humienik, M.; Możejko, J. Kinetics of thermal decomposition of $ZnSO_4 \cdot 7H_2O$. *Thermochim. Acta* **1997**, *292*, 145–150. [CrossRef]
26. Lin, F.; Yang, S. The study of the dehydrating mechanism of zinc sulfate heptahydrate. *J. Chongqing Norm. Uni.* **2006**, *23*, 55–57.
27. Saha, J.; Podder, J. Crystallization of zinc sulphate single crystals and its structural, thermal and optical characterization. *J. Bangladesh Acad. Sci.* **2011**, *35*, 203–210. [CrossRef]
28. Attia, S.; Hevroni, L.; Danon, A.; Meyerstein, D.; Koresh, J.E.; Finkelstein, Y. The role of the cation in the oxygen isotopic exchange in crystalline sulfate salt hydrates. *Adsorption* **2013**, *19*, 821–833. [CrossRef]
29. Carsky, M.; Veselý, V.; Hartman, M.; Haluza, J. Dehydration of zinc sulphate in a fluidised bed drier. *S. Afr. J. Chem. Eng.* **2014**, *19*, 1–8.
30. Yang, W.; Jun, Y. Gibbs free energy minimization and TG-DTA analysis for thermal decomposition of zinc sulfate heptahydrate. *Inorg. Chem. Ind.* **2014**, *46*, 31–33.
31. Höffler, F.; Müller, I.; Steiger, M. Thermodynamic properties of $ZnSO_4$ (aq) and phase equilibria in the $ZnSO_4$ –H_2O system from 268 K to 373 K. *J. Chem. Thermodyn.* **2018**, *116*, 279–288. [CrossRef]
32. Rehman, A.U.; Maosheng, Z.; Hayat, A. Hydration performance and cycling stability of threeTCM:$MgSO_4$, $ZnSO_4$ and $FeSO_4$. *Int. J. Energy Res.* **2020**, *44*, 6981–6990. [CrossRef]
33. Liu, H.; Chen, G.-M.; Ma, J.; Fan, Y.-X.; Tao, Z.-Y. Zinc sulfate hydrates characterization by terahertz time domain spectroscopy. *Optik* **2022**, *253*, 168594. [CrossRef]
34. Rego, A.S.C.; Navarro, R.C.S.; Brocchi, E.A.; Souza, R.F.M. Kinetic modeling of the thermal decomposition of zinc sulfate through a global optimization method. *Metall. Mater. Trans. B* **2022**, *53*, 4105–4113. [CrossRef]
35. Bertouche, S.; Tomao, V.; Ruiz, K.; Hellal, A.; Boutekedjiret, C.; Chemat, F. First approach on moisture determination in food products using alpha-pinene as an alternative solvent for Dean–Stark distillation. *Food Chem.* **2012**, *134*, 602–605. [CrossRef]
36. Moya, M.; Sánchez, D.; Romero, J.Á.; Villar-García, J.R. Influence of Moisture Content on Some Mechanical Properties of Wheat. *Agronomy* **2024**, *14*, 347. [CrossRef]
37. Sivakumar, A.; Sahaya Jude Dhas, S.; Elberin Mary Theras, J.; Jose, M.; Sivaprakash, P.; Arumugam, S.; Martin Britto Dhas, S.A. Spectroscopic and diffraction studies of polycrystalline copper sulfate pentahydrate at shocked conditions. *Solid State Sci.* **2021**, *121*, 106751. [CrossRef]
38. Yuvaraj, M.; Subramanian, K.S. Development of slow release Zn fertilizer using nano-zeolite as carrier. *J. Plant Nutr.* **2018**, *41*, 311–320. [CrossRef]
39. Fan, Y.; Xue, R.; Chen, F. Explanation and prediction for the product of trehalose dihydrate selective dehydration process using mid-frequency Raman difference spectra. *Vib. Spectrosc.* **2024**, *130*, 103626. [CrossRef]
40. Koskela, J.; Sutton, J.J.; Lipiäinen, T.; Gordon, K.C.; Strachan, C.J.; Fraser-Miller, S.J. Low- versus mid-frequency Raman spectroscopy for in situ analysis of crystallization in slurries. *Mol. Pharm.* **2022**, *19*, 2316–2326. [CrossRef]
41. Robert, C.; Fraser-Miller, S.J.; Berzins, K.; Okeyo, P.O.; Rantanen, J.; Rades, T.; Gordon, K.C. Monitoring the isothermal dehydration of crystalline hydrates using low-frequency Raman spectroscopy. *Mol. Pharm.* **2021**, *18*, 1264–1276. [CrossRef] [PubMed]
42. Fan, Y.; Liang, C.; Li, Y.; Xiao, W.; Niu, Y.; Jin, H.; Xue, R.; Chen, F. Explanation and prediction of the selective crystallization of boscalid by mid-frequency Raman difference spectroscopy analysis. *CrystEngComm* **2023**, *25*, 3548–3555. [CrossRef]
43. Zhang, Y.-H.; Chan, C.K. Understanding the hygroscopic properties of supersaturated droplets of metal and ammonium sulfate solutions using Raman spectroscopy. *J. Phys. Chem. A* **2002**, *106*, 285–292. [CrossRef]
44. Hayes, A.C.; Kruus, P.; Adams, W.A. Raman spectroscopic study of aqueous $(NH_4)_2SO_4$ and $ZnSO_4$ solutions. *J. Sol. Chem.* **1984**, *13*, 61–75. [CrossRef]
45. Kurban, G.V.T.; Rego, A.S.C.; Mello, N.M.; Brocchi, E.A.; Navarro, R.C.S.; Souza, R.F.M. Thermodynamics and kinetic modeling of the $ZnSO_4 \cdot H_2O$ thermal decomposition in the presence of a Pd/Al_2O_3 catalyst. *Energies* **2022**, *15*, 548. [CrossRef]

46. Pandey, R.; Pourhashem, G.; Gladen, A.C. Screening of salt hydrates and cellulose nanocrystal composites for thermochemical energy storage using life cycle assessment. *Sustainable Mater. Technol.* **2024**, *40*, e00889. [CrossRef]
47. Blake, A.J.; Cooke, P.A.; Hubberstey, P.; Sampson, C.L. Zinc(II) sulfate tetrahydrate. *Acta Crystallogr. Sect. E Struct. Rep. Online* **2001**, *57*, i109–i111. [CrossRef]

Disclaimer/Publisher's Note: The statements, opinions and data contained in all publications are solely those of the individual author(s) and contributor(s) and not of MDPI and/or the editor(s). MDPI and/or the editor(s) disclaim responsibility for any injury to people or property resulting from any ideas, methods, instructions or products referred to in the content.